Published in final edited form as:

Circ Arrhythm Electrophysiol. 2015 August ; 8(4): 942–950. doi:10.1161/CIRCEP.114.002162.

Feedback Mechanisms for Cardiac-Specific microRNAs and cAMP Signaling in Electrical Remodeling

Richard Myers, PhD[1], **Valeriy Timofeyev, PhD**[1], **Ning Li, PhD**[1], **Catherine Kim, BS**[1], **Hannah A. Ledford, BS**[1], **Padmini Sirish, PhD**[1], **Victor Lau, BS**[1], **Yinuo Zhang**[1], **Kiran Fayyaz, BS**[1], **Anil Singapuri, MS**[1], **Javier E. Lopez, MD**[1], **Anne A. Knowlton, MD**[1,2], **Xiao-Dong Zhang, PhD**[1], and **Nipavan Chiamvimonvat, MD**[1,2]

[1]Division of Cardiovascular Medicine, University of California, Davis

[2]Department of Veterans Affairs, Northern California Health Care System, Mather, CA

Abstract

Background—Loss of transient outward K^+ current (I_{to}) is well documented in cardiac hypertrophy and failure both in animal models and humans. Electrical remodeling contributes to prolonged action potential duration (APD) and increased incidence of arrhythmias. Furthermore, there is a growing body of evidence linking microRNA (miR) dysregulation to the progression of both conditions. In this study, we examined the mechanistic basis underlying miR dysregulation in electrical remodeling and revealed a novel interaction with the adrenergic signaling pathway.

Methods and Results—We first employed a tissue-specific knockout model of *Dicer1* in cardiomyocytes to reveal the overall regulatory effect of miRs on the ionic currents and action potentials. We then validated the inducible cAMP early repressor (ICER) as a target of *miR-1* and took advantage of a clinically relevant model of post myocardial infarction (MI) and miR delivery to probe the mechanistic basis of miR dysregulation in electrical remodeling. These experiments revealed the role of ICER as a repressor of *miR-1* and I_{to}, leading to prolonged APD post MI. In addition, delivery of *miR-1 and miR-133a* suppressed ICER expression and prevented both electrical remodeling and hypertrophy.

Conclusions—Taken together, our results illuminate the mechanistic links between miRs, adrenergic signaling, and electrical remodeling. They also serve as a proof-of-concept for the therapeutic potential of miR delivery post MI.

Keywords

microRNA; ion channel; adrenergic stimulation; myocardial infarction; remodeling; electrical remodeling

Correspondence: Nipavan Chiamvimonvat, Division of Cardiovascular Medicine, Department of Medicine, University of California, Davis, One Shields Avenue, GBSF 6315, Davis, CA 95616, Tel: (530) 754-7158, Fax: (530) 754-7167, nchiamvimonvat@ucdavis.edu. Xiao-Dong Zhang, Division of Cardiovascular Medicine, Department of Medicine, University of California, Davis, One Shields Avenue, GBSF 6315, Davis, CA 95616, Tel: (530) 754-7158, Fax: (530) 754-7167, xdzhang@ucdavis.edu.

Conflict of Interest Disclosures: None

Introduction

MicroRNAs (miRs) are endogenously expressed, non-coding RNAs of ~22 nucleotides (nts) in length.[1] When processed by the ribonuclease III (RNase III) enzyme, DICER1, and incorporated into the RNA-induced silencing complex (RISC), they target a variety of coding messenger RNAs (mRNAs) for degradation and translational repression.[2] In cardiac hypertrophy and failure, the cardiomyocyte-specific *miR-1* and *miR-133a* are dramatically reduced.[3,4] These miRs are co-transcribed from a common gene and together have been ascribed critical regulatory roles in hypertrophy,[3,5,6] apoptosis,[7,8] fibrosis,[9] and ion channel expression.[10–14] *MiR-1*, in particular, has been shown to enhance the transient outward K^+ current (I_{to}) by repressing iroquois homeobox domain 5 (IRX5), a transcriptional inhibitor of $K_V4.2$ (*Kcnd2*), the main pore-forming subunit for I_{to}, and loss of *miR-1* may underlie the I_{to} remodeling seen post myocardial infarction (MI).[12,15,16]

In the acute phase of MI, levels of *miR-1* and *miR-133a* increase and can be detected in the circulation.[17] However, these *miRs* quickly decline,[18,19] and lead to chronically depressed levels.[20] Myocardia from patients with ischemic heart failure exhibited decreased levels of *miR-1* and *miR-133a* which were restored after implantation of a left ventricular assist device (LVAD).[21] In a separate study, loss of DICER1 reported in the end-stage heart failure patients was similarly rescued by LVAD implantation.[22]

A recent study has identified the presence of a cAMP response element (CRE) sequence in the *miR-1/133a* promoter region,[23] implicating a potential role for β-adrenergic signaling in the regulation of miR expression. In addition, cAMP response element modulator (CREM) is a predicted target of *miR-1*. CREM acts as a regulator of cAMP response element binding protein (CREB) signaling.[24] Both proteins are activated by β-adrenergic signaling and compete for binding to the CRE in gene promoters.[25,26] One isoform of CREM, termed the inducible cAMP early repressor (ICER), arises from an alternative internal promoter and is induced by β-adrenergic signaling.[27] ICER contains only the CRE DNA binding domain and acts as a powerful repressor of CREB signaling. Under physiological conditions, ICER acts in a negative feedback fashion to prevent over activation of CREB-dependent genes. Under chronic pathological conditions, excessive β-adrenergic signaling drives a progressive increase in ICER expression that may contribute to inhibition of CREB-dependent gene expression and β-adrenergic desensitization.[28,29] Recent studies have documented the beneficial effects of preserving β-adrenergic sensitivity after an MI[30,31] and knockout of CREM was shown to be protective under chronic β-adrenergic signaling.[32] In addition, cardiac-specific knockout of CREB led to electrical remodeling in cardiomyocytes similar to that seen post MI with a loss of I_{to} and prolonged action potential durations (APDs).[33]

Electrical remodeling has been well documented in cardiac hypertrophy and failure with down-regulation of K^+ currents and APD prolongation.[34] Moreover, recent studies have provided strong evidence for the critical roles of miRs in ion channel regulation.[10–14] In addition, loss of miRs may underlie the well documented electrical remodeling seen in pathological cardiac hypertrophy and failure.[12,15,16] However, the mechanistic basis leading to miRs dysregulation with significant loss of *miR-1/133a* in diseased conditions remains incompletely understood.

Since the promoter region of cardiac-specific *miR-1/133a* contains the CRE sequence, we hypothesize that chronic cAMP signaling may underlie miRs dysregulation. Specifically, we hypothesize that under pathological conditions, chronic over-expression of ICER from excessive β-adrenergic signaling[28,29] may repress *miR-1* expression leading to the well documented electrical remodeling. To test the hypothesis, we first examined the roles of miRs in the regulation of cardiac excitability by taking advantage of a knockout model of *Dicer1* and cardiac delivery of Cre Recombinase. This model allowed us to directly test the roles of miRs on ionic currents without the interference of organ level changes such as hypertrophy or fibrosis. We then investigated the relationship between *miR-1/133a*, cAMP signaling, and electrical remodeling in a clinically relevant mouse model of MI. Indeed, we documented that *Icer* mRNA is significantly increased in the MI model. We further demonstrated that chronic isoproterenol (ISO) infusion results in similar up-regulation of *Icer* mRNA. *In vivo* delivery of miRs was used to directly establish the relationship between *miR-1/133a* and ICER. Expression of ICER is normalized after delivery of *miRs* in both the MI and chronic ISO infusion models. Moreover, we directly validate both CREM and ICER as the targets of *miR-1* establishing a feedback mechanism between cardiac-specific miRs and cAMP signaling. Our study uncovers novel mechanisms of interactions between cardiac-specific *miRs*, pathological cAMP signaling post MI, and their possible roles in pro-arrhythmic electrical remodeling.

Methods

Detailed Materials and Methods are presented in the Supplemental Material. All animal care and procedures were approved by the University of California, Davis, Institutional Animal Care and Use Committee. Animal care and use was in accordance with National Institutes of Health and institutional guidelines.

Neonatal Mouse Cardiomyocyte Culture

Cardiomyocytes from 1–3 days old neonatal *Dicer1*^{tm1Bdh}*/J* were isolated by enzymatic digestion using trypsin as described in the Supplemental Material.

Intramyocardial Adenovirus Injection

C57 BL/6J and *Dicer1*^{tm1Bdh}*/J* mice (8–12 weeks) were anesthetized. Recombinant adenovirus (50–100 μl) containing Cre-recombinase (Cre) and green fluorescence protein (GFP) (Ad-GFP-Cre) was delivered *via* intramyocardial injection to the left ventricular free wall. Cardiomyocytes were isolated 2 weeks after the injection. Transduced cells were identified based on GFP fluorescence. *Dicer1*^{tm1Bdh}*/J* mice injected with Ad-GFP served as additional controls.

Myocardial Infarction Mouse Model

Ischemia-reperfusion model of myocardial infarction was performed as previously published.[35–37] C57 BL/6J mice (10–16 weeks) were prepared and the heart exposed to reveal the left anterior descending coronary artery (LAD). The LAD was then ligated for 45 minutes and allowed to reperfuse.

In Vivo miR Injections

Mmu-miR-1 and miR-133a mimics (*Dharmacon C-310377, C-310408*) were packaged as using MaxSuppressor *in vivo* RNA-LANCEr II (*Biooscientific 3410-01*) and delivered together *via* tail vein injections 1 week after LAD surgery at 30 μg per 28g mouse. Non-silencing MiR Mimic Transfection Control with and without Dy547 (*Dharmacon CP-004500-01*) was injected in control animals.

In Vivo Mouse Model of Isoproterenol Infusion

In vivo isoproterenol (ISO) infusion at a dose of 30 mg/kg/day in C57 BL/6J mice (10–16 weeks) was performed using Alzet osmotic mini-pumps for 6 hours, 2, 4, and 14 days.[38] Sham littermate animals received osmotic mini-pumps loaded with saline alone.

Analysis of Cardiac Function by Echocardiography

Echocardiograms using M-mode and two-dimensional (2D) measurements to assess systolic function were performed as described previously.[37]

Electrocardiographic (ECG) Recordings

ECG recordings were obtained at 33°C using Bioamplifier (BMA 831, CWE, Incorporated, Ardmore, PA) as previously described.[39] A total of 100 beats were analyzed from each animal in a blinded fashion. The rate-corrected QT interval (QT_c) was calculated using modified Bazett's formula as reported by Mitchell et al for mouse models, whereby the RR interval was first expressed as a unitless ratio (RR in ms/100 ms). QT_c interval was defined as (QT interval (in ms)/$(RR/100)^{1/2}$).[40]

Adult Mouse Cardiomyocyte Isolation

Single mouse LV myocytes were isolated as previously described.[41] The cells were then enriched for cardiomyocytes. Final cell populations were determined to be 95% myocytes as measured by flow cytometry (Figure S1, Supplemental Material).

Patch-Clamp Recordings

Whole-cell and perforated patch clamp recordings were performed as previously described.[41,42]

Flow Cytometric Analysis

Flow cytometric analysis of isolated mouse cells was performed as described.[37]

Quantitative Real-Time PCR (qRT-PCR)

RNA was isolated from adherent neonatal and dissociated adult cardiomyocytes. qRT-PCR was performed using RT^2 SYBR Green Master Mix (*Qiagen 330520*) and the Viia™ 7 Real Time PCR System (*ABI*).

Immunofluorescence Confocal Microscopy

Immunofluorescence confocal microscopy was performed as previously described.[43,44]

miR-1 Target Validation using Luciferase Assay and Western Blot Analysis

Luciferase assay was performed using the Dual-Light® Luciferase & β-Galactosidase Reporter Gene Assay System (Life Technologies T1003). Additional validation was performed using western blot analysis.

Statistical Analyses

Significant difference between groups was determined using Origin Pro 7 software by One-Way ANOVA and validated by Bonferroni, Sheffe, and Tukey tests with an $n \geq 3$ at $p < 0.05$ unless otherwise noted.

Results

A Loss of DICER1 Results in Electrical Remodeling Independent of Cardiac Hypertrophy and Failure

Mouse hearts subjected to ischemia-reperfusion (IR) displayed decreased levels of *Dicer1* mRNA (Figure 1a). To directly determine if a loss of DICER1 alone without concomitant cardiac hypertrophy can result in electrical remodeling of cardiac ionic currents and action potentials, we delivered a Cre Recombinase expressing adenovirus (Ad-GFP-Cre) to the left ventricles of *Dicer1*^{tm1Bdh}*/J* mice (Figure 1b) that contain a floxed RNase III domain critical for DICER1 function.[45] This model allowed us to directly test the roles of miRs on ionic currents without the interference of organ level changes such as hypertrophy or fibrosis. Patch-clamp analyses were performed using isolated ventricular myocytes Knockout of *Dicer1* in adult mouse cardiomyocytes led to prolonged action potential duration (APD) (Figure 1c) resulting from decreased transient outward K^+ current (I_{to}) (Figure1d) and increased Ca^{2+} currents (I_{Ca}) (Figure1e).

Parallel experiments were performed using cardiomyocytes isolated from neonatal *Dicer1*^{tm1Bdh}*/J* mice. Cells were transduced 48 hours after isolation with Ad-GFP-Cre or Ad-GFP for experimental and control groups, respectively, at a multiplicity of infection (MOI) of 10–50. Myocytes were cultured for a total of 7 days and subjected to patch-clamp recording of I_{to} currents and RT-PCR analyses. Figure 2a shows immunofluorescence confocal images of neonatal cardiomyocytes transduced with Ad-GFP and Ad-GFP-Cre. Cre recombinase (red) can be detected in the nuclei of Ad-GFP-Cre cells. Furthermore, RT-PCR products show expression of Cre transcripts in Ad-GFP-Cre transfected cells (Figure 2b). Knockout of *Dicer* resulted in increased and decreased transcripts for $Ca_V1.2$ (*Cacna1c*) and $K_V4.2$ (*Kcnd2*), respectively (Figure 2c). Patch-clamp analyses further demonstrated a significant down-regulation of I_{to} (Figure 2d) in *Dicer* knockout cardiomyocytes. Moreover, there was a significant increase in the expression of the known *Kcnd2* transcriptional inhibitor, iroquois homeobox domain 5 (IRX5), a validated target of *miR-1*[12,15,16] (Figure 2c).

Crem and *Icer* are Targets of *miR-1*

Using microRNA.org and miRwalk databases, we identified CREM, as well as its two ICER isoforms, as potential targets of *miR-1* with a mirSVR score of −1.2211. To directly validate CREM and ICER as *miR-1* targets, we first identified the predicted *miR-1* binding sequence

to be present in the 3' UTRs of all CREM isoforms except CREM7 and 8, which correspond to τ-like isoforms not found in the heart[46] (Figure 3**a**). Importantly, the *miR-1* binding sequence was found in the two ICER isoforms of CREM (Figure 3a). The conserved sequence (*Crem*) and scramble sequence (scramble) were subcloned into luciferase reporter vectors (Figure S2**a**, Supplemental Material). Luciferase assays were then performed using a *miR-1* mimic compared to a non-silencing control miR. A vector expressing β-galactosidase served as a loading control for normalization. *MiR-1* treatment induced a dose-dependent decrease in luminescence in the crem-transfected cells (Figure S2**b–c**, Supplemental Material). Crem-transfected cells displayed a 77% decrease in luminescence with *miR-1* treatment (1 pmol) compared to the control miR (Figure 2**b–c**, Supplemental Material). No change from control was observed with *miR-1* treatment in cells transfected with the scramble sequence or empty vector.

We further validated CREM and ICER as *miR-1* target at the protein level using western blot analysis (Figure S2d). HEK 293 cells were transfected with a plasmid containing human *Crem*. Cells were then treated with *miR-1* mimic compared to a non-silencing control miR. Western blot analysis was performed using anti-CREM and anti-β-tubulin antibodies demonstrating a significant reduction in the level of CREM protein in cells treated with *miR-1* mimic compared to non-silencing control (Figure S2d, Supplemental Material).

Delivery of *miR-1/133a* Preserves Left Ventricular Function and Prevents Hypertrophy after MI

We took advantage of *in vivo* delivery of *miR-1* and the co-transcribed *miR-133a* to directly test the roles of *miR-1* and *-133* on the long-term electrical remodeling after an MI. The optimization of *miR-1/133a* delivery was first performed in HEK 293 cells (Figure S3, Supplemental Material). We employed a clinically relevant model of ischemia/reperfusion (IR) surgery in wild-type C57 mice where the left ascending coronary artery (LAD) was ligated for 45 minutes and then allowed to reperfuse (Figure S4**a**, Supplemental Material). We reason that this model accurately represents the clinical situation where occluded coronary arteries are rapidly revascularized. In both the IR model and in patients, the long-term effects of MI include hypertrophy, fibrosis, electrical remodeling, and progression toward heart failure.

Echocardiographic recordings one week after IR surgery revealed decreased fractional shortening (FS) and increased left ventricular end systolic diameter (LVESD) (Figures 4**c** and S4b, Supplemental Material). Mice were then randomized to receive *miR-1* and *miR-133a* packaged in a neutral lipid emulsion (NLE) by tail vein injections or control non-silencing miR (Figure 4a–b). Three weeks after IR surgery, FS continued to decline in MI mice receiving the control injection (MI control) while MI mice that received the *miR-1/133a* injection (MI+miRs) displayed a significant improvement in FS (**P*<0.05, Figures 4c &S3). MI control mice also exhibited increased in heart weight / body weight (HW/BW) ratio (Figure 4d) and demonstrated increased transcripts of atrial natriuretic peptide (*Nppa*) and angiotensinogen (*Agt*) (Figure 4d). In all cases, hypertrophy was prevented in the MI miR mice (Figure 2d, HW/BW ratio) and levels for *Nppa* and *Agt* returned to the sham levels (Figure 4d). Angiotensinogen (AGT) is a predicted target of

miR-133a and local release of AGT has been described as pathological in MI.[47] *Nppa* and skeletal α-actin (*Acta1*) are not predicted targets of *miR-1* nor *miR-133a* but their expression has been linked to both miRs through indirect mechanisms.[6,9]

Delivery of *miR-1/133a* Prevents Electrical Remodeling after MI

To directly test the roles of *miR-1* and *133a* on electrical remodeling, we performed patch-clamp recordings of I_{to}, I_{Ca}, and APD on isolated cardiomyocytes. In MI mice, peak I_{to} current was significantly reduced (Figure 5a), leading to prolonged APD (Figure 5b). Moreover, delivery of *miR-1* and *-133a* resulted in the recovery of peak I_{to} density towards the sham levels (Figure 5a) together with normalization of the voltage-dependent activation of I_{to} towards sham control (Figure S5, Supplemental Material, $^*P<0.05$). Indeed, after MI, there were a 35% decrease in $K_V4.2$ channel transcripts (*Kcnd2*) and a 77% increase in *Irx5* (Figure 6a). *MiR-1/133a* delivery prevented the increase in *Irx5* expression and increased *Kcnd2* levels to 85% of sham levels (Figure 6a). In addition, consistent with to the findings observed after *Dicer* knockout (Figure 1e), peak I_{Ca} density (Figure S6, Supplemental Material) elicited at +10 mV was significantly reduced by miR delivery.

ICER is Increased in MI and Chronic Isoproterenol Infusion Models and the Expression of ICER is Normalized after the Delivery of *miRs* in Both Models

Using a primer specific to ICER isoforms, we found that *Icer* mRNA increased >2-fold in MI control mice, consistent with previous studies which demonstrate that *Icer* can be activated by β-adrenergic signaling.[25,26] More importantly, the level of *Icer* returned to the sham levels with miR delivery (Figure 6b). Using a primer that recognizes all isoforms of *Crem* except for *Icer*, we found that non-*Icer Crem* mRNA did not increase in MI control but that miR delivery decreased expression by 60% in both sham+miR and MI+miR mice. *Creb* expression decreased slightly with MI but was not affected by miR delivery.

To directly test the roles of β-adrenergic signaling on the expression of ICER and miRs in the heart, we took advantage of the second mouse model with chronic isoproterenol (ISO) infusion. Transcript levels of *Icer*, *Creb*, *Kcnd2*, *miR-1* and *-133* were assessed from cardiac myocytes (Figure S7a). Chronic ISO challenge resulted in a significant increase in *Icer* mRNA similar to the post MI model with a corresponding decrease in *Kcnd2* and *miR-1*. The effects of ISO on the up-regulation of *Icer* mRNA occurred as early as 6 hours and lasted up to 2 weeks in our study (Figure S7a). More importantly, similar to the MI model, treatment with *miR-1/133a* by tail vein injections normalized the levels of *Icer* (Figure S7b). We directly documented a significant increase in heart rate as measured using RR intervals (Figure S7c) in the chronic ISO infusion model.

Discussion

Even though significant loss of miRs has previously been documented in pathological cardiac hypertrophy and failure,[12,15,16] the underlying mechanisms for the miR dysregulation remain incompletely understood. The current study directly tests the hypothesis that chronic over-expression of ICER from excessive β-adrenergic signaling[28,29] may repress *miR-1* expression leading to the well documented electrical remodeling. First,

by taking advantage of a knockout model of *Dicer1* in the heart, we demonstrated the direct regulation of cardiac excitability by *miRs*. We further confirmed that *miR-1* directly targets and represses the expression of CREM and ICER. The level of ICER expression is increased during pathological conditions such as post MI. Moreover, chronic ISO stimulation induces a similar increase in ICER expression supporting the roles of β-adrenergic stimulation in the up-regulation of ICER. By using *in vivo* delivery of miRs, we directly establish the relationship between *miR-1/133a* and the expression of ICER. Finally, our study provides a tantalizing proof-of-concept for the therapeutic potential of miR delivery post MI.

Possible Feedback Mechanism Between *miR-1/133a*, cAMP Response Elements, and Electrical Remodeling

In the post MI model, chronic β-adrenergic stimulation is predicted to result in the overexpression of ICER which leads to long-term suppression of *miR-1* and *miR-133a*. Indeed, using a chronic ISO infusion, we directly document a significant increase in ICER expression by β-adrenergic stimulation. A decrease in *miR-1* leads to a further increase in ICER level. Moreover, exogenous delivery of *miR-1* results in the normalization of ICER levels in both models (Figures 6b and S7b).

Loss of *miR-1* leads to overexpression of IRX5, loss of $K_v4.2$ and I_{to}, and prolonged APDs. Loss of *miR-133a* leads to increased AGT expression and hypertrophy. Indeed, the delivery of cardiac-specific miRs can restore the level of ICER towards the control. Taken together, the results in our study suggest a feedback mechanism between *miR-1/133a*, cAMP response elements, and electrical remodeling in pathological conditions with heightened βAR stimulation (Figure 6c).

Roles of CREM and ICER in the Heart

Consistent with our hypothesis, recent studies have shown that prevention of β-adrenergic desensitization after an MI can improve ejection fraction and survivability while decreasing cardiac hypertrophy and apoptosis.[30,31] It has been demonstrated that cardiac-specific knockout of CREM prevented hypertrophy, fibrosis, and LV dysfunction associated with chronic β-adrenergic signaling.[32] Conversely, cardiac-driven ICER and CREM overexpression led to increased apoptosis and progressive mortality.[48] Moreover, cardiac-specific knockout of CREB led to a 50% reduction in $K_v4.2$ resulting in a significant loss of peak I_{to} and prolonged APDs even though the $K_v4.2$ promoter appears to lack a CRE sequence.[33] Our findings demonstrating that both CREM and ICER are direct targets of *miR-1* may help explain these earlier results. Moreover, increased expression of ICER post MI leads to a reduction of *miR-1* and *-133* and the consequences of electrical remodeling.

Knockout of *Dicer1* driven by the α-MHC promoter has been shown to result in increased mortality, hypertrophy, dilated cardiomyopathy (DCM), increased fibrosis and apoptosis, and remodeling of gap junction proteins.[12,22] The mechanism of DICER1 loss seen in heart failure and post MI remains elusive, though evidence suggests it may be a response to stresses in failing hearts which are relieved by the LVADs. Further evidence of a stress-dependent mechanism come from experiments in culture that show a loss of Dicer

expression in a variety of cell types in response to treatment with reactive oxygenated species (ROS) via H_2O_2, interferons, or serum withdrawal.[49,50]

Clinical Implications and Future Studies

Electrical remodeling in cardiac hypertrophy and failure can predispose patients to malignant arrhythmias and sudden cardiac death. Our study reveals novel mechanisms underlying electrical remodeling *via* the dysregulation of miRs and implicates ICER as a potential therapeutic target. At the translational level, our study provides a molecular basis for the potential roles for *miR-1* and *-133a* therapy post MI and offers a proof-of-concept for miR intervention. Future studies are required to further dissect and quantify the beneficial effects of miR delivery on cardiac remodeling including the degree of cardiac fibrosis and apoptosis.

In the current study, miR delivery was performed one week post MI. However, at 3 weeks of follow-up, ICER level remains elevated (Figure 6b). Therefore, we expect miR delivery to reduce ICER level and possibly prevent further remodeling and provide beneficial outcomes. Nonetheless, additional studies are required to test whether this strategy may be applicable to pre-existing MI with substantial remodeling as well as the long-term beneficial effects of miR intervention.

Supplementary Material

Refer to Web version on PubMed Central for supplementary material.

Acknowledgments

The authors would like to acknowledge the contributions of the following people to this study: Bert Frederich, Jonathan Nguyen, Jasmine Bibay, Joseph Chen, Simranjeet Benipal, Elisa Zhang, and Sin Mei Ma.

Funding Sources: Supported by NIH/NHLBI (R01 HL075274 and R01 HL085844 to NC), VA Merit Review Grant I01 BX000576 (to NC), American Heart Association Beginning Grant-in-Aid (to XZ), and American Heart Association Predoctoral Fellowship Award (to PS). PS received Postdoctoral Fellowship from NIH/NHLBI Institutional Training Grant in Basic and Translational Cardiovascular Science (T32 NIH HL086350). NC is the holder of the Roger Tatarian Endowed Professor in Cardiovascular Medicine.

References

1. Lee RC, Feinbaum RL, Ambros V. The C. elegans heterochronic gene lin-4 encodes small RNAs with antisense complementarity to lin-14. Cell. 1993; 75:843–854. [PubMed: 8252621]
2. Gregory RI, Chendrimada TP, Cooch N, Shiekhattar R. Human RISC couples microRNA biogenesis and posttranscriptional gene silencing. Cell. 2005; 123:631–640. [PubMed: 16271387]
3. Sayed D, Hong C, Chen IY, Lypowy J, Abdellatif M. MicroRNAs play an essential role in the development of cardiac hypertrophy. Circ Res. 2007; 100:416–424. [PubMed: 17234972]
4. van Rooij E, Sutherland LB, Liu N, Williams AH, McAnally J, Gerard RD, Richardson JA, Olson EN. A signature pattern of stress-responsive microRNAs that can evoke cardiac hypertrophy and heart failure. Proc Natl Acad Sci U S A. 2006; 103:18255–18260. [PubMed: 17108080]
5. Liu N, Bezprozvannaya S, Williams AH, Qi X, Richardson JA, Bassel-Duby R, Olson EN. microRNA-133a regulates cardiomyocyte proliferation and suppresses smooth muscle gene expression in the heart. Genes Dev. 2008; 22:3242–3254. [PubMed: 19015276]
6. Care A, Catalucci D, Felicetti F, Bonci D, Addario A, Gallo P, Bang ML, Segnalini P, Gu Y, Dalton ND, Elia L, Latronico MV, Hoydal M, Autore C, Russo MA, Dorn GW 2nd, Ellingsen O, Ruiz-

Lozano P, Peterson KL, Croce CM, Peschle C, Condorelli G. MicroRNA-133 controls cardiac hypertrophy. Nat Med. 2007; 13:613–618. [PubMed: 17468766]

7. Xu C, Lu Y, Pan Z, Chu W, Luo X, Lin H, Xiao J, Shan H, Wang Z, Yang B. The muscle-specific microRNAs miR-1 and miR-133 produce opposing effects on apoptosis by targeting HSP60, HSP70 and caspase-9 in cardiomyocytes. J Cell Sci. 2007; 120:3045–3052. [PubMed: 17715156]
8. He B, Xiao J, Ren AJ, Zhang YF, Zhang H, Chen M, Xie B, Gao XG, Wang YW. Role of miR-1 and miR-133a in myocardial ischemic postconditioning. J Biomed Sci. 2011; 18:22. [PubMed: 21406115]
9. Matkovich SJ, Wang W, Tu Y, Eschenbacher WH, Dorn LE, Condorelli G, Diwan A, Nerbonne JM, Dorn GW 2nd. MicroRNA-133a protects against myocardial fibrosis and modulates electrical repolarization without affecting hypertrophy in pressure-overloaded adult hearts. Circ Res. 2010; 106:166–175. [PubMed: 19893015]
10. Xiao J, Luo X, Lin H, Zhang Y, Lu Y, Wang N, Yang B, Wang Z. MicroRNA miR-133 represses HERG K+ channel expression contributing to QT prolongation in diabetic hearts. J Biol Chem. 2007; 282:12363–12367. [PubMed: 17344217]
11. Luo X, Xiao J, Lin H, Li B, Lu Y, Yang B, Wang Z. Transcriptional activation by stimulating protein 1 and post-transcriptional repression by muscle-specific microRNAs of IKs-encoding genes and potential implications in regional heterogeneity of their expressions. J Cell Physiol. 2007; 212:358–367. [PubMed: 17443681]
12. da Costa Martins PA, Bourajjaj M, Gladka M, Kortland M, van Oort RJ, Pinto YM, Molkentin JD, De Windt LJ. Conditional dicer gene deletion in the postnatal myocardium provokes spontaneous cardiac remodeling. Circulation. 2008; 118:1567–1576. [PubMed: 18809798]
13. Yang B, Lin H, Xiao J, Lu Y, Luo X, Li B, Zhang Y, Xu C, Bai Y, Wang H, Chen G, Wang Z. The muscle-specific microRNA miR-1 regulates cardiac arrhythmogenic potential by targeting GJA1 and KCNJ2. Nat Med. 2007; 13:486–491. [PubMed: 17401374]
14. Girmatsion Z, Biliczki P, Bonauer A, Wimmer-Greinecker G, Scherer M, Moritz A, Bukowska A, Goette A, Nattel S, Hohnloser SH, Ehrlich JR. Changes in microRNA-1 expression and IK1 up-regulation in human atrial fibrillation. Heart Rhythm. 2009; 6:1802–1809. [PubMed: 19959133]
15. Costantini DL, Arruda EP, Agarwal P, Kim KH, Zhu Y, Zhu W, Lebel M, Cheng CW, Park CY, Pierce SA, Guerchicoff A, Pollevick GD, Chan TY, Kabir MG, Cheng SH, Husain M, Antzelevitch C, Srivastava D, Gross GJ, Hui CC, Backx PH, Bruneau BG. The homeodomain transcription factor Irx5 establishes the mouse cardiac ventricular repolarization gradient. Cell. 2005; 123:347–358. [PubMed: 16239150]
16. He W, Jia Y, Takimoto K. Interaction between transcription factors Iroquois proteins 4 and 5 controls cardiac potassium channel Kv4.2 gene transcription. Cardiovasc Res. 2009; 81:64–71. [PubMed: 18815185]
17. Cheng C, Wang Q, You W, Chen M, Xia J. MiRNAs as Biomarkers of Myocardial Infarction: A Meta-Analysis. PLoS One. 2014; 9:e88566. [PubMed: 24533109]
18. Dimmeler S, Zeiher AM. Circulating microRNAs: novel biomarkers for cardiovascular diseases? Eur Heart J. 2010; 31:2705–2707. [PubMed: 20605798]
19. Zile MR, Mehurg SM, Arroyo JE, Stroud RE, DeSantis SM, Spinale FG. Relationship between the temporal profile of plasma microRNA and left ventricular remodeling in patients after myocardial infarction. Circ Cardiovasc Genet. 2011; 4:614–619. [PubMed: 21956146]
20. Bostjancic E, Zidar N, Stajer D, Glavac D. MicroRNAs miR-1, miR-133a, miR-133b and miR-208 are dysregulated in human myocardial infarction. Cardiology. 2010; 115:163–169. [PubMed: 20029200]
21. Schipper ME, van Kuik J, de Jonge N, Dullens HF, de Weger RA. Changes in regulatory microRNA expression in myocardium of heart failure patients on left ventricular assist device support. J Heart Lung Transplant. 2008; 27:1282–1285. [PubMed: 19059107]
22. Chen JF, Murchison EP, Tang R, Callis TE, Tatsuguchi M, Deng Z, Rojas M, Hammond SM, Schneider MD, Selzman CH, Meissner G, Patterson C, Hannon GJ, Wang DZ. Targeted deletion of Dicer in the heart leads to dilated cardiomyopathy and heart failure. Proc Natl Acad Sci U S A. 2008; 105:2111–2116. [PubMed: 18256189]

23. Lu Y, Zhang Y, Shan H, Pan Z, Li X, Li B, Xu C, Zhang B, Zhang F, Dong D, Song W, Qiao G, Yang B. MicroRNA-1 downregulation by propranolol in a rat model of myocardial infarction: a new mechanism for ischaemic cardioprotection. Cardiovasc Res. 2009; 84:434–441. [PubMed: 19581315]
24. Foulkes NS, Borrelli E, Sassone-Corsi P. CREM gene: use of alternative DNA-binding domains generates multiple antagonists of cAMP-induced transcription. Cell. 1991; 64:739–749. [PubMed: 1847666]
25. Ruppert S, Cole TJ, Boshart M, Schmid E, Schutz G. Multiple mRNA isoforms of the transcription activator protein CREB: generation by alternative splicing and specific expression in primary spermatocytes. EMBO J. 1992; 11:1503–1512. [PubMed: 1532935]
26. Laoide BM, Foulkes NS, Schlotter F, Sassone-Corsi P. The functional versatility of CREM is determined by its modular structure. EMBO J. 1993; 12:1179–1191. [PubMed: 8458330]
27. Molina CA, Foulkes NS, Lalli E, Sassone-Corsi P. Inducibility and negative autoregulation of CREM: an alternative promoter directs the expression of ICER, an early response repressor. Cell. 1993; 75:875–886. [PubMed: 8252624]
28. Ma D, Fu L, Shen J, Zhou P, Gao Y, Xie R, Li Y, Han Y, Wang Y, Wang F. Interventional effect of valsartan on expression of inducible cAMP early repressor and phosphodiesterase 3A in rats after myocardial infarction. Eur J Pharmacol. 2009; 602:348–354. [PubMed: 19027736]
29. Tomita H, Nazmy M, Kajimoto K, Yehia G, Molina CA, Sadoshima J. Inducible cAMP early repressor (ICER) is a negative-feedback regulator of cardiac hypertrophy and an important mediator of cardiac myocyte apoptosis in response to beta-adrenergic receptor stimulation. Circ Res. 2003; 93:12–22. [PubMed: 12791704]
30. White DC, Hata JA, Shah AS, Glower DD, Lefkowitz RJ, Koch WJ. Preservation of myocardial beta-adrenergic receptor signaling delays the development of heart failure after myocardial infarction. Proc Natl Acad Sci U S A. 2000; 97:5428–5433. [PubMed: 10779554]
31. Bathgate-Siryk A, Dabul S, Pandya K, Walklett K, Rengo G, Cannavo A, De Lucia C, Liccardo D, Gao E, Leosco D, Koch WJ, Lymperopoulos A. Negative impact of beta-arrestin-1 on post-myocardial infarction heart failure via cardiac and adrenal-dependent neurohormonal mechanisms. Hypertension. 2014; 63:404–412. [PubMed: 24218435]
32. Muller FU, Lewin G, Matus M, Neumann J, Riemann B, Wistuba J, Schutz G, Schmitz W. Impaired cardiac contraction and relaxation and decreased expression of sarcoplasmic Ca2+-ATPase in mice lacking the CREM gene. FASEB J. 2003; 17:103–105. [PubMed: 12475904]
33. Schulte JS, Seidl MD, Nunes F, Freese C, Schneider M, Schmitz W, Muller FU. CREB critically regulates action potential shape and duration in the adult mouse ventricle. Am J Physiol Heart Circ Physiol. 2012; 302:H1998–H2007. [PubMed: 22427515]
34. Nass RD, Aiba T, Tomaselli GF, Akar FG. Mechanisms of disease: ion channel remodeling in the failing ventricle. Nat Clin Pract Cardiovasc Med. 2008; 5:196–207. [PubMed: 18317475]
35. Tarnavski O, McMullen JR, Schinke M, Nie Q, Kong S, Izumo S. Mouse cardiac surgery: comprehensive techniques for the generation of mouse models of human diseases and their application for genomic studies. Physiol Genomics. 2004; 16:349–360. [PubMed: 14679301]
36. Li N, Liu JY, Timofeyev V, Qiu H, Hwang SH, Tuteja D, Lu L, Yang J, Mochida H, Low R, Hammock BD, Chiamvimonvat N. Beneficial effects of soluble epoxide hydrolase inhibitors in myocardial infarction model: Insight gained using metabolomic approaches. J Mol Cell Cardiol. 2009; 47:835–845. [PubMed: 19716829]
37. Sirish P, Li N, Liu JY, Lee KS, Hwang SH, Qiu H, Zhao C, Ma SM, Lopez JE, Hammock BD, Chiamvimonvat N. Unique mechanistic insights into the beneficial effects of soluble epoxide hydrolase inhibitors in the prevention of cardiac fibrosis. Proc Natl Acad Sci U S A. 2013; 110:5618–5623. [PubMed: 23493561]
38. Oudit GY, Crackower MA, Eriksson U, Sarao R, Kozieradzki I, Sasaki T, Irie-Sasaki J, Gidrewicz D, Rybin VO, Wada T, Steinberg SF, Backx PH, Penninger JM. Phosphoinositide 3-kinase gamma-deficient mice are protected from isoproterenol-induced heart failure. Circulation. 2003; 108:2147–2152. [PubMed: 12963636]

39. Zhang Z, Xu Y, Song H, Rodriguez J, Tuteja D, Namkung Y, Shin HS, Chiamvimonvat N. Functional Roles of Cav1.3 (a1D) calcium channel in sinoatrial nodes: insight gained using gene-targeted null mutant mice. Circ Res. 2002; 90:981–987. [PubMed: 12016264]
40. Mitchell GF, Jeron A, Koren G. Measurement of heart rate and Q-T interval in the conscious mouse. Am J Physiol. 1998; 274:H747–H751. [PubMed: 9530184]
41. Timofeyev V, Myers RE, Kim HJ, Woltz RL, Sirish P, Heiserman JP, Li N, Singapuri A, Tang T, Yarov-Yarovoy V, Yamoah EN, Hammond HK, Chiamvimonvat N. Adenylyl cyclase subtype-specific compartmentalization: differential regulation of L-type Ca2+ current in ventricular myocytes. Circ Res. 2013; 112:1567–1576. [PubMed: 23609114]
42. Hamill OP, Marty A, Neher E, Sakmann B, Sigworth FJ. Improved patch-clamp techniques for high-resolution current recording from cells and cell-free membrane patches. Pflugers Arch. 1981; 391:85–100. [PubMed: 6270629]
43. Lu L, Timofeyev V, Li N, Rafizadeh S, Singapuri A, Harris TR, Chiamvimonvat N. Alpha-actinin2 cytoskeletal protein is required for the functional membrane localization of a Ca2+-activated K+ channel (SK2 channel). Proc Natl Acad Sci U S A. 2009; 106:18402–18407. [PubMed: 19815520]
44. Rafizadeh S, Zhang Z, Woltz RL, Kim HJ, Myers RE, Lu L, Tuteja D, Singapuri A, Bigdeli AA, Harchache SB, Knowlton AA, Yarov-Yarovoy V, Yamoah EN, Chiamvimonvat N. Functional interaction with filamin A and intracellular Ca2+ enhance the surface membrane expression of a small-conductance Ca2+-activated K+ (SK2) channel. Proc Natl Acad Sci U S A. 2014; 111:9989–9994. [PubMed: 24951510]
45. Harfe BD, McManus MT, Mansfield JH, Hornstein E, Tabin CJ. The RNaseIII enzyme Dicer is required for morphogenesis but not patterning of the vertebrate limb. Proc Natl Acad Sci U S A. 2005; 102:10898–10903. [PubMed: 16040801]
46. Foulkes NS, Mellstrom B, Benusiglio E, Sassone-Corsi P. Developmental switch of CREM function during spermatogenesis: from antagonist to activator. Nature. 1992; 355:80–84. [PubMed: 1370576]
47. Schunkert H, Ingelfinger JR, Hirsch AT, Tang SS, Litwin SE, Talsness CE, Dzau VJ. Evidence for tissue-specific activation of renal angiotensinogen mRNA expression in chronic stable experimental heart failure. J Clin Invest. 1992; 90:1523–1529. [PubMed: 1401084]
48. Muller FU, Lewin G, Baba HA, Boknik P, Fabritz L, Kirchhefer U, Kirchhof P, Loser K, Matus M, Neumann J, Riemann B, Schmitz W. Heart-directed expression of a human cardiac isoform of cAMP-response element modulator in transgenic mice. J Biol Chem. 2005; 280:6906–6914. [PubMed: 15569686]
49. Wiesen JL, Tomasi TB. Dicer is regulated by cellular stresses and interferons. Mol Immunol. 2009; 46:1222–1228. [PubMed: 19118902]
50. Asada S, Takahashi T, Isodono K, Adachi A, Imoto H, Ogata T, Ueyama T, Matsubara H, Oh H. Downregulation of Dicer expression by serum withdrawal sensitizes human endothelial cells to apoptosis. Am J Physiol Heart Circ Physiol. 2008; 295:H2512–H2521. [PubMed: 18978195]

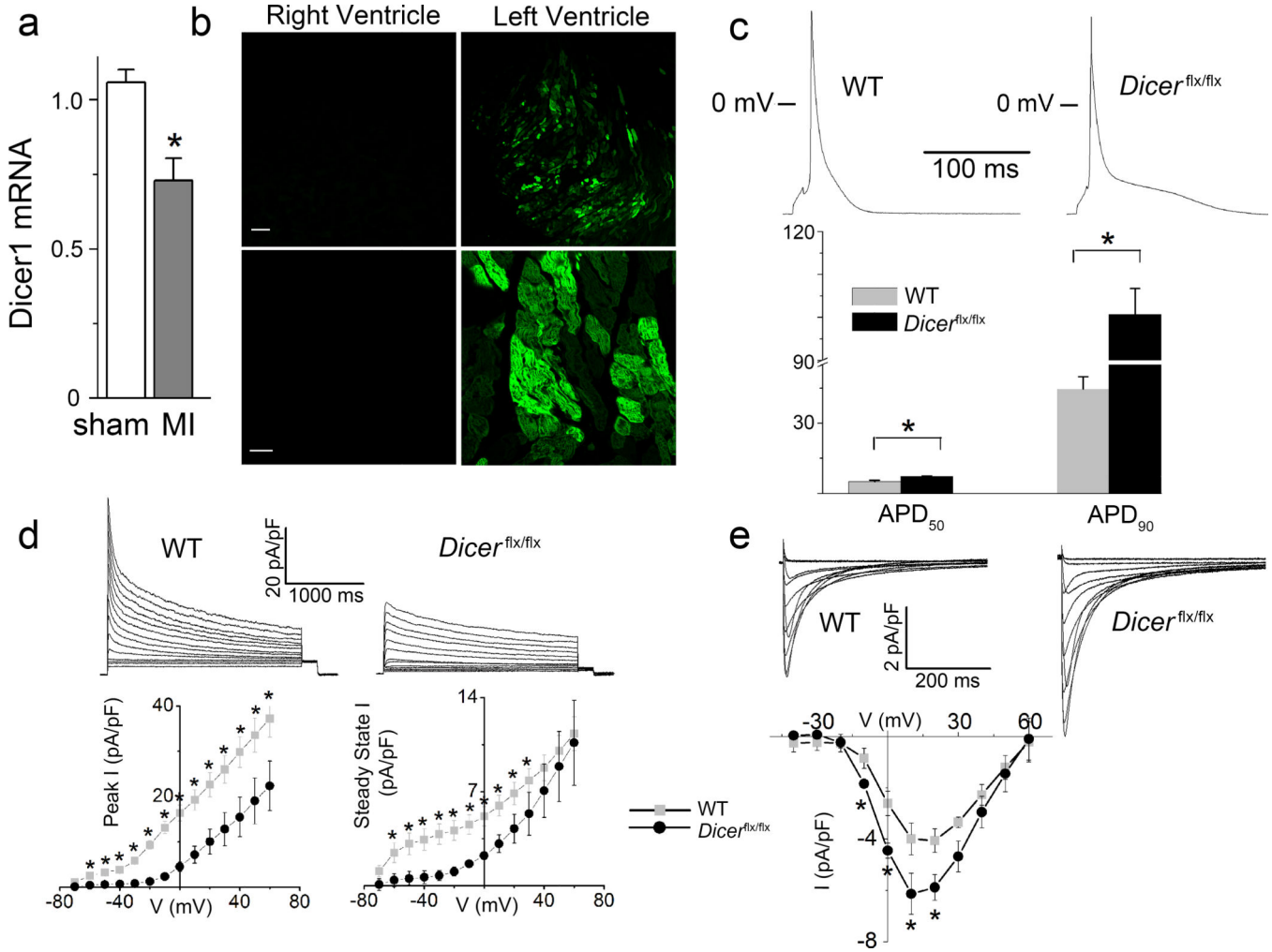

Figure 1.

Dicer Knockout Leads to Electrical Remodeling in Adult Cardiomyocytes (a) qRT-PCR results normalized to GAPDH expression from sham and MI mice for *Dicer1* mRNA (*n=3*, **p<0.05*). (b) Paraffin sections of a *Dicer*$^{flx/flx}$ mouse heart after Ad-GFP-Cre injection showing GFP expression at the injection site at low magnification (*scale = 100 μm*) and high magnification (*scale = 20 μm*). (c) Action potentials recorded from left ventricular cardiomyocytes isolated from WT compared to *Dicer*$^{flx/flx}$ mice using a stimulation frequency of 0.1 Hz. Cardiomyocytes which were transduced with Ad-GFP-Cre were identified using GFP fluorescence. Lower panel shows summary data of APD at 50 and 90% of repolarization (APD_{50} and APD_{90}, *n=8* for each group, **p<0.05*). (d) Examples of I_{to} recorded from left ventricular myocytes isolated from WT and *Dicer*$^{flx/flx}$ mice. I_{to} was elicited from a holding potential of −80 mV using a family of voltage steps from −70 to +60 mV with 10-mV increment and 2.5 seconds in duration. The interpulse interval was 10 seconds. Lower panels show the summary data for the current-voltage relations for the peak and steady-state currents (*n=7* for each groups, **p<0.05*). (e) Examples of I_{Ca} recorded from left ventricular myocytes isolated from adult WT and *Dicer*$^{flx/flx}$ mice. I_{Ca} was elicited from a holding potential of −55 mV using a family of voltage steps from −40 to +60 mV with 10-

mV increment and 500 ms in duration. The interpulse interval was 5 seconds. Lower panel shows the summary data for the current-voltage relations (n=5 for WT and 10 for *Dicer*$^{flx/flx}$ mice, respectively, *$p<0.05$).

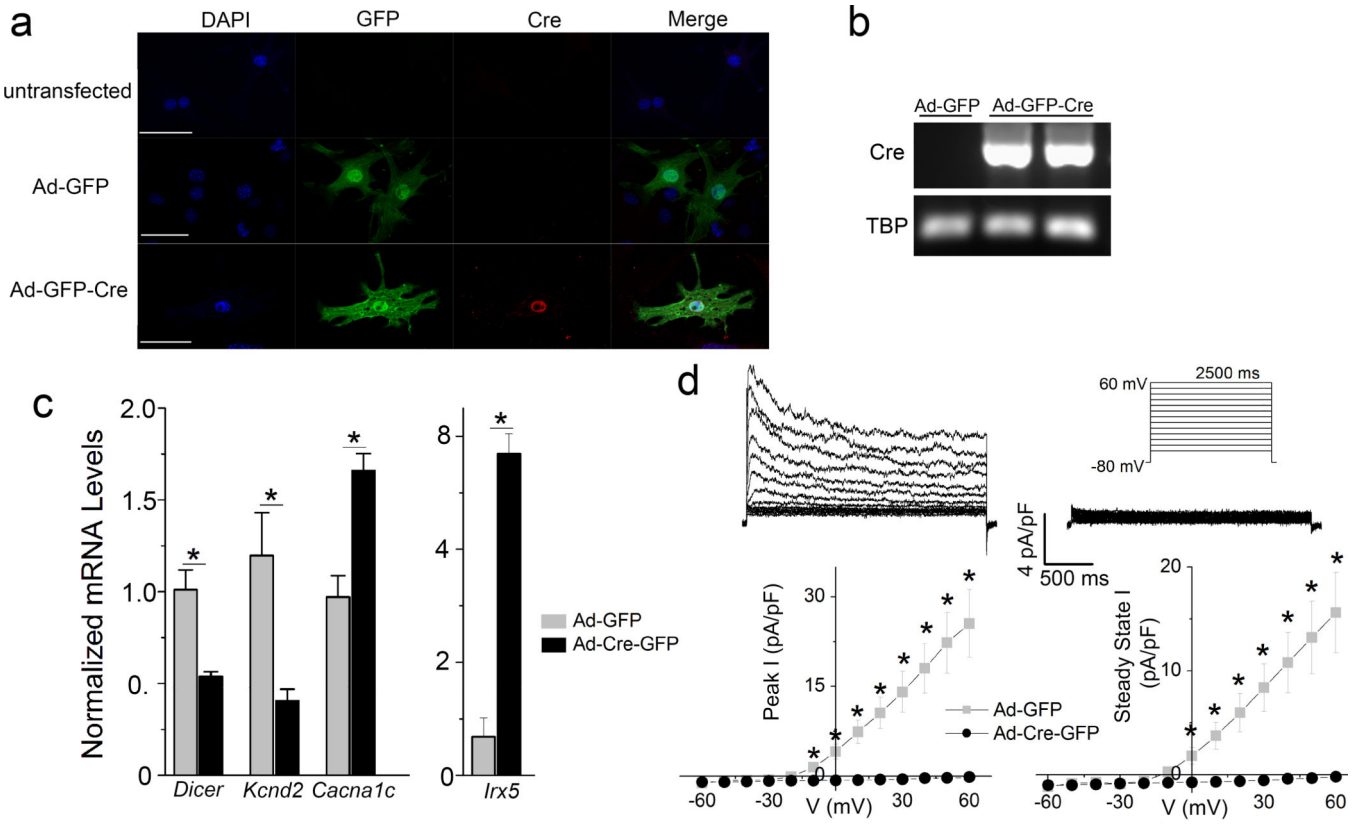

Figure 2.

Dicer Knockout Leads to Electrical Remodeling in Neonatal Cardiomyocytes (a) Immunofluorescence confocal images of neonatal cardiomyocytes transduced with Ad-GFP and Ad-GFP-Cre. Cre recombinase (red) is seen in the nucleus of Ad-GFP-Cre cells. GFP expression (green) is seen in transfected cells (*scale = 50 μm*). (b) RT-PCR products show Cre transcripts in Ad-GFP-Cre transfected cells. (c) qRT-PCR results normalized to GAPDH expression and relative to Ad-GFP treated controls (*n=3, *p<0.05*). (d) I_{to} currents recorded from neonatal cardiomyocytes transduced with Ad-GFP (left panel) compared to cardiomyocytes transduced with Ad-GFP-Cre (right panel). I_{to} was elicited using the same protocol as in Figure 1. Lower panels show the summary data for current-voltage relations from peak and steady-state component comparing cardiomyocytes transduced with Ad-GFP or Ad-GFP-Cre (*n=6* cells for each group, **p<0.05*).

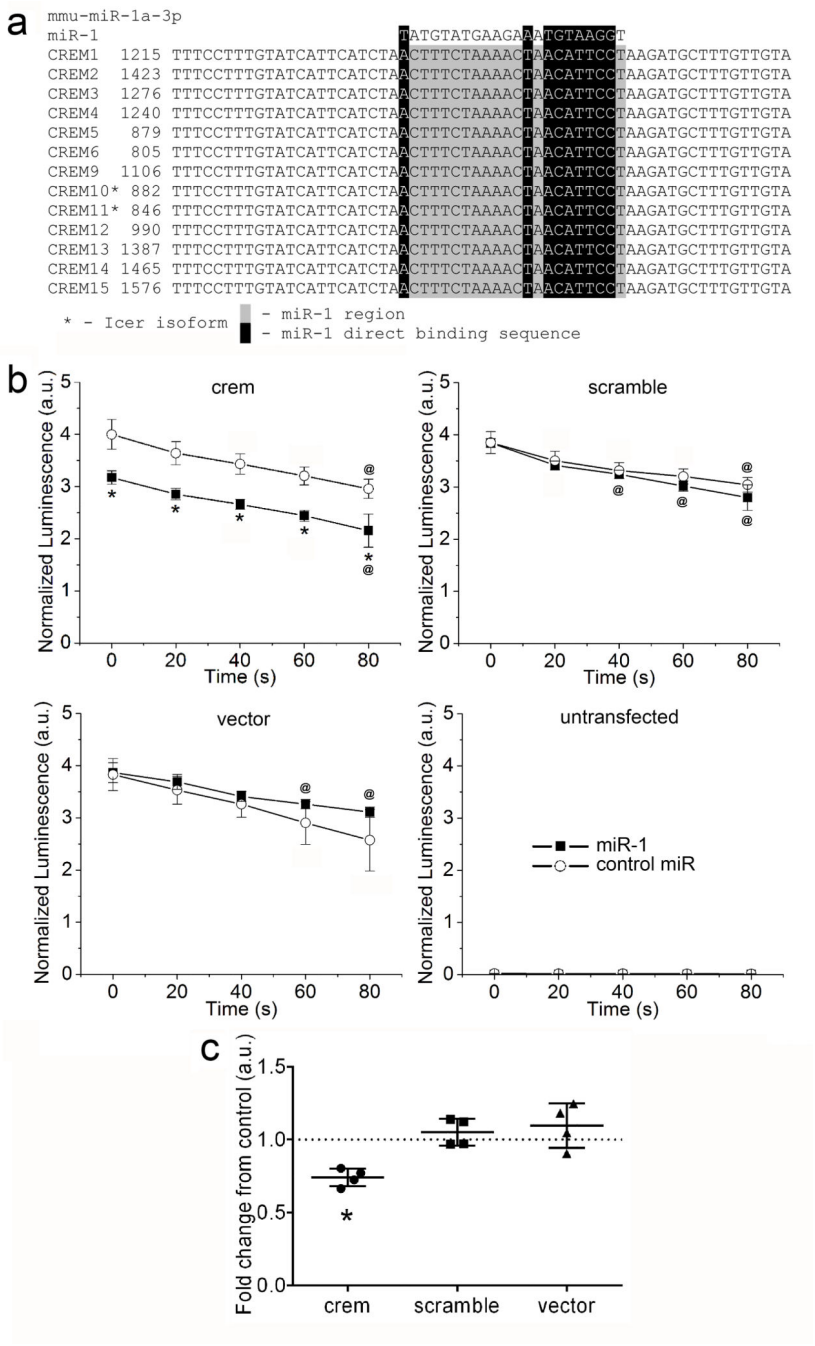

Figure 3.

Validation of *Icer* and *Crem* as *miR-1* Targets (a) Alignment of *miR-1* sequence with the predicted target sequences in crem isoforms. (b) Time course of luciferase signals in cells transfected with *Crem* or scramble inserts and treated with either *miR-1* or control miR mimics. Cells transfected with the original vector served as a positive control and untransfected cells served as a negative control. Luciferase intensity was normalized by β-galactoside signal. (c) Fold change between *miR-1* and control miR treatment in cells transfected with *Crem*, scramble, or vector constructs. Values were normalized to control

miR intensity and made relative to vector values for comparison ($n=4$, $*p<0.05$). Correlations over time were also calculated against values at time = 0 second ($^{@}p\leq 0.05$). These changes reflected the decay of the luciferase signals with time and were consistent among all groups including cells transfected with *Crem*, scramble, or vector constructs and treated with *miR-1* or control miR.

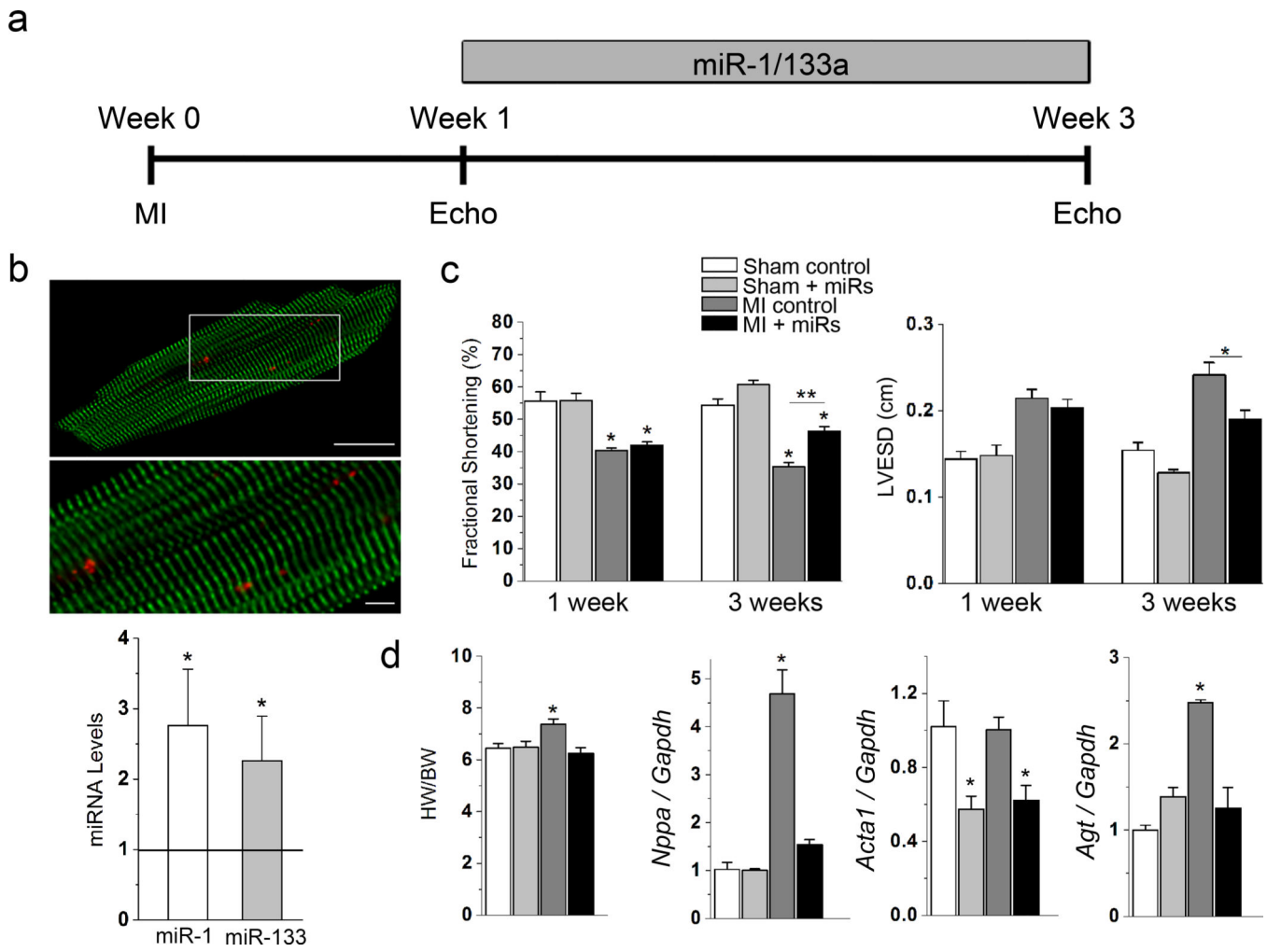

Figure 4.

miR-1/133a Delivery Preserves Left Ventricular Function and Prevents Hypertrophy after MI (a) Experimental time course for echocardiography and *miR-1/133a* delivery relative to MI surgery. (b) Cardiomyocytes isolated from adult mice 3 days after tail vein injection of 30 μg of Dy547-labelled *miR-1/133* (red) with α-actinin staining (green) (scale = 50 μm (top) and 10 μm (bottom)). Lower panel shows qRT-PCR demonstrating increased *miR-1* and *miR-133a* in the same cells. (c) Calculated average fraction shortening and average measurements for left ventricular end-systolic diameter (LVESD) at 1 week and 3weeks after MI ($n=5$, $*p<0.05$). (d) Heart weight/body weight ratio (HW/BW) and average mouse body weight ($n=5$, $*p<0.05$). qRT-PCR results normalized to GAPDH expression and relative to sham controls ($n=3$, $*p<0.05$).

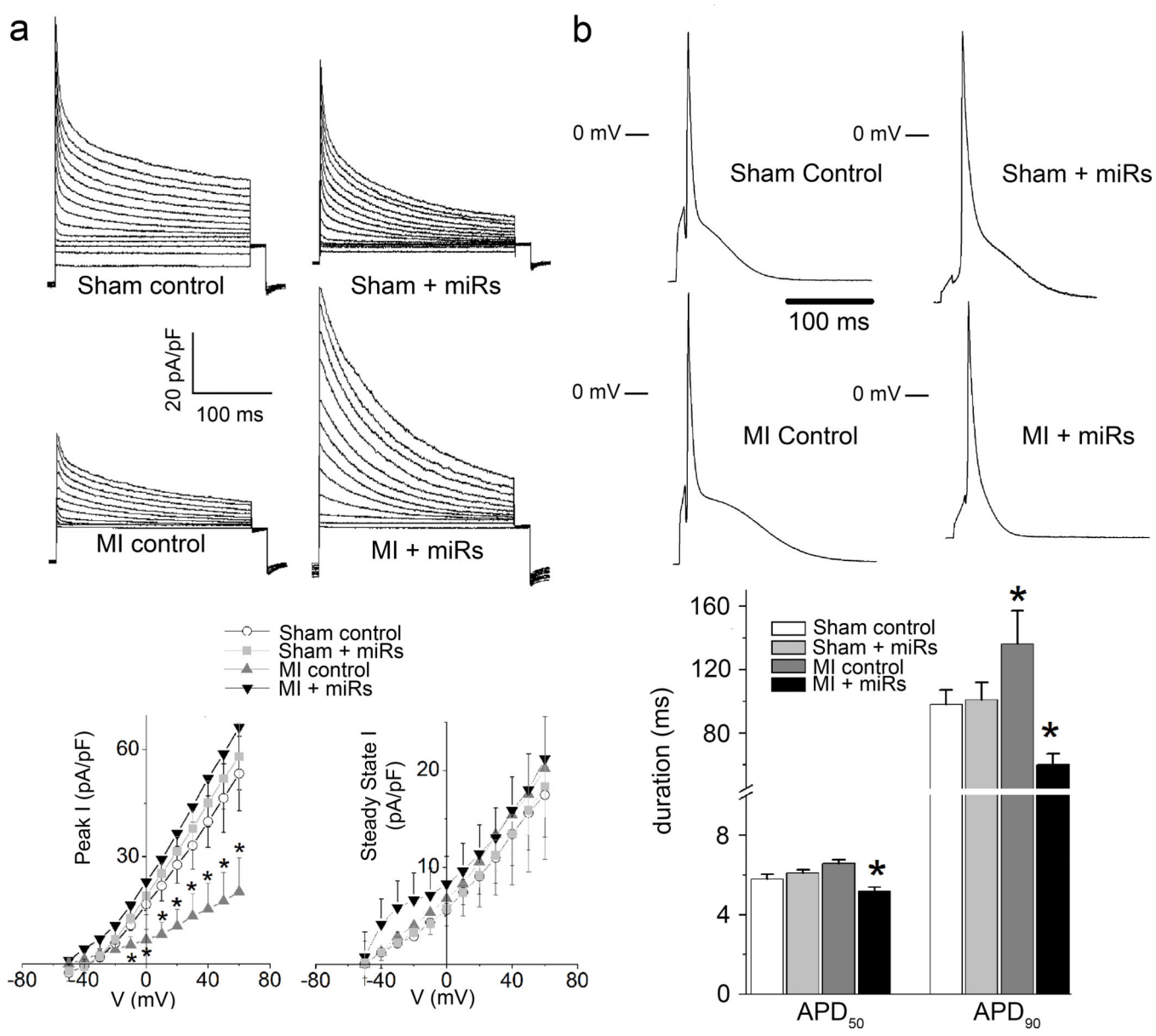

Figure 5.

miR-1/133a Delivery Prevents I_{to} Remodeling APD Prolongation after MI (a) Representative I_{to} traces from sham and MI mice after tail vein injection of *miR-1/133* mimics or control miR using the same voltage-clamp protocol as in Figure 1. Lower panels show summary data for the peak and steady-state current-voltage relationships (*n=9–11* for each group, **p<0.05*). (b) Representative AP recordings of sham and MI mice after tail vein injection of *miR-1/133* mimics or control miR. Lower panel shows the summary data for APD_{50} and APD_{90} (*n=6–8* for each group, **p<0.05*).

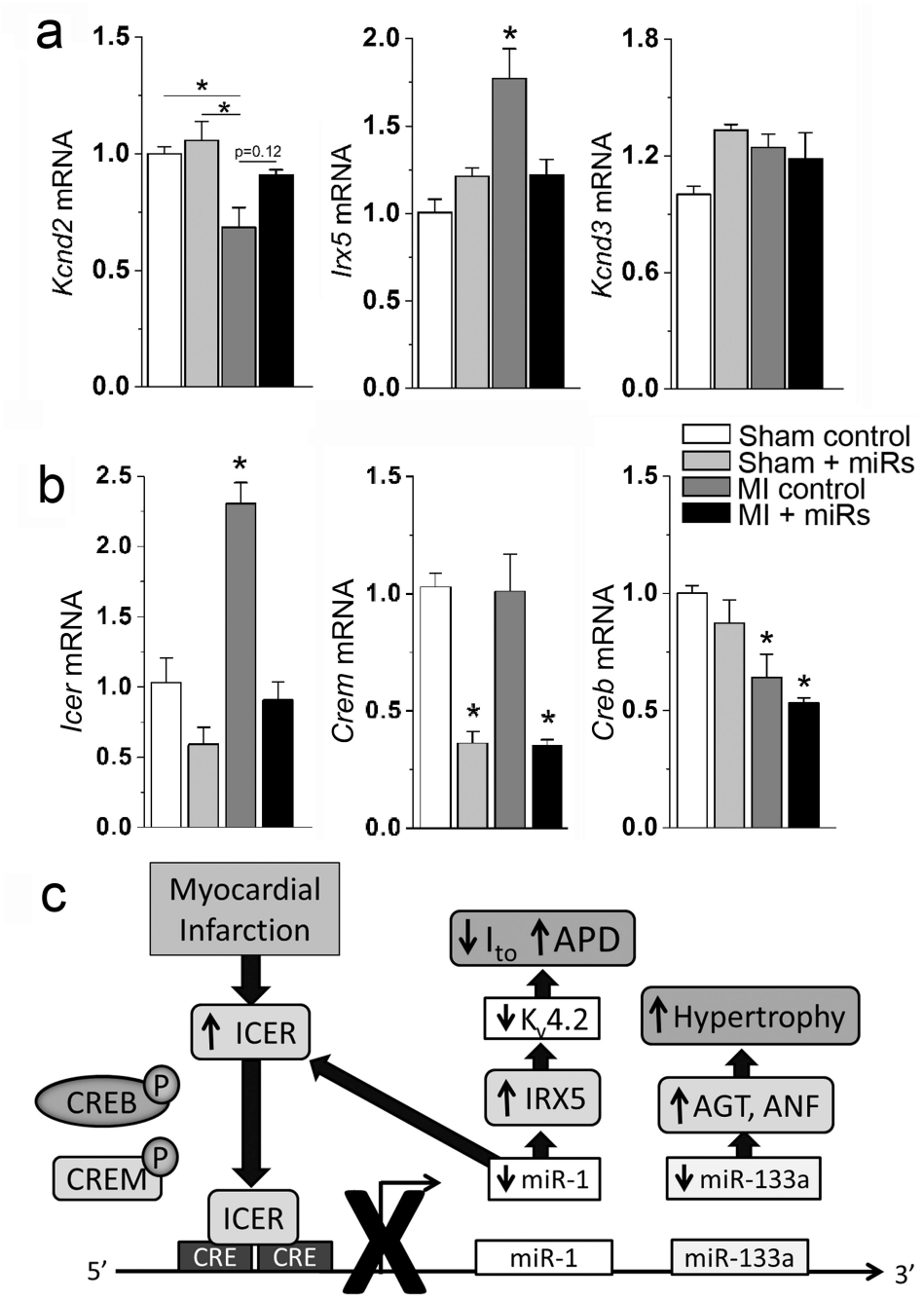

Figure 6.

miR-1/133a Delivery Prevents Remodeling of $K_V4.2$ and ICER after MI (a) qRT-PCR results normalized to GAPDH expression and relative to sham controls for *Kcnd2*, *Irx5*, and *Kcnd3* (*n=3, *p<0.05*). (b) qRT-PCR results for *Icer*, *Crem*, and *Creb* expression in mice (*n=3, *p<0.05*). (c) Schematic representation of the role of ICER signaling on *miR-1/133a* during MI.